Experimental tests on masonry strengthened with bed joint reinforced repointing

L. Licciardello, J.G. Rots, R. Esposito
Delft University of Technology, the Netherlands

Bed joint reinforced repointing, also known as bed joint reinforcement, is a strengthening method often used in the Netherlands to counteract settlement damage. It consists in the installation of twisted steel bars in mortar joint embedded in high-strength repair mortar. Currently it is of interest to investigate whether this strengthening technique is efficient against induced seismic load, since the gas extraction from the subsoil is causing an increase of the induced seismic events in the region of Groningen, in the northern part of the country.

In order to characterize the performance of the bed joint reinforced repointing using twisted steel bars, an experimental campaign was conducted at Delft University of Technology. A quasi-static cyclic in-plane test on a full-scale wall and four-point bending tests on masonry wallets were performed; similar tests on unstrengthened specimens were available from a previous experimental campaign and they were used for comparison. Moreover, small scale pull-out tests were performed to study the interaction between the steel bars and the repair mortar.

The bed joint reinforcement results efficient in reducing crack width and crack length up to the serviceability limit state; the performance of strengthened masonry at near collapse show an increase in terms of ductility and displacement capacity for the wall subject to in-plane loading. The preliminary information obtained for the presented case study provides the ground for further research as well as benchmark for numerical modelling.

Keywords: Unreinforced masonry (URM), settlement, induced seismicity, bed joint reinforcement, twisted steel bars, experimental tests

1 Introduction

The bed joint reinforced repointing (in Dutch “lintvoegwapening”) consists of cutting a slot in the mortar joint, with a depth of approximately 1/3 of its thickness and to install the reinforcement (steel, stainless steel, FRP bars) embedded in a high-strength repair mortar. This technique does not influence the aesthetic aspect of the building and it can be applied with limited invasiveness, in this way the historical and the artistic aspects are preserved. In the Netherlands, the buildings' stock is mainly composed of unreinforced masonry and the bed joint reinforcement is often used as strengthening method to counteract settlement damage. Moreover, during the last years the phenomena of the induced seismicity considerably increased due to the gas extraction from the subsoil in the region of Groningen (northern part of the Netherlands), causing problems to the masonry buildings since they were not designed accordingly to seismic criteria. Therefore, it is of interest to investigate the performance of unreinforced masonry strengthened with bed joint reinforced repointing under settlement and seismic load.

Previous studies on reinforced repointing mainly focused on evaluating its effectiveness against settlement and creep damage, while less attention has been paid to the seismic performance of masonry strengthened with bed joint reinforcement. Previous researchers (Valluzzi et al. 2005, NIKER 2010) showed no significant improvement of the strength of masonry, but thanks to the confining action provided by the bed joint reinforcement a reduction of the dilation and a reduced cracks pattern were obtained. In literature, limited information on the seismic performance of masonry strengthened with bed joint reinforcement is available. In this respect, researchers mainly performed diagonal-shear compression tests on wallets. Ismail et al. (2011) made a comparison of the bed joint reinforcement with a near-surface mounted technique made by placing steel bars in the vertical direction, being this often done to prevent out-of-plane failure of unreinforced masonry buildings in countries prone to strong intensity seismic events.

To this purpose an experimental campaign was conducted at Delft University of Technology; a quasi-static cyclic in-plane test on a full-scale wall and four point bending tests on unstrengthened and strengthened masonry wallets were performed to study the efficiency of the bed joint reinforced repointing against seismic load and settlement, respectively (Drougkas et al. 2020a, Drougkas et al. 2020b, Licciardello and Esposito 2020, Licciardello et al. 2021). The experimental results obtained from the test on the

strengthened specimens are compared with the results obtained on similar unstrengthened ones from previous experimental campaigns (Korswagen et al. 2017, Korswagen et al. 2018). Section 2 provides a detailed description of the material used, the type of specimen, the tests set-up and the loading protocols. Section 3 shows the main results that were obtained from the unstrengthened and the strengthened specimens. The results are discussed in section 4 and Section 5 presents the main concluding remarks.

2 Materials and methods

The tests aim to assess the performance of the bed joint reinforced repointing with twisted steel bars against seismic load and settlement. For this purpose, both in-plane tests on full-scale walls and small-scale four-point bending tests on wallets were performed on strengthened masonry and compared with previously obtained results for unstrengthened masonry (Korswagen et al. 2017, Korswagen et al. 2018). Additionally, a complete mechanical characterisation of the adopted materials and of the bond-slip behaviour of the twisted bars is provided.

2.1 Description of the specimens

To study the seismic performances of masonry strengthened with bed joint reinforcement, the results of quasi-static cyclic in-plane tests on a full-scale walls with opening were considered (Figure 1a). Two different walls were used: a pre-damaged and subsequently strengthened wall (TUD-COMP-45) and an undamaged and unstrengthened wall (TUD_COMP-41) (Korswagen et al. 2017, Korswagen et al. 2018, Messali 2018). Both the walls had dimensions equal to 3070 x 2690 x 100 mm with a window opening of 780 x 1510 x 100 mm; the opening was placed asymmetric leading to the presence of a narrow pier P1 and a wider pier P2 (where the term pier is here adopted to define portion of masonry located next to the window and having the same height of the opening). A prefabricated concrete lintel (980 x 50 x 100 mm) was built at the top of the window. This wall typology is typical of detached house, which is a common residential typology in the Netherlands (Kallioras et al. 2018). To evaluate the response of the wall for low intensity and repetitive earthquakes, typical of the Groningen area, two cyclic protocols were applied: one to evaluate the response up to the light damage phase (phase 1 and 2) and one to evaluate the response up to near collapse (phase 3). In the light damage phase, a maximum crack width of approximately 2 mm was reached (Korswagen et al. 2017, Korswagen et al. 2018). To reproduce the damage caused by settlement before an earthquake, the wall TUD_COMP-

45 was pre-damaged by creating un-bonded brick-joint interfaces using thin plastic strips (orange lines in Figure 1a). The wall TUD_COMP-45 was firstly tested up to light damage state, (light blue lines in Figure 1a) and then strengthened with bed joint reinforced repointing. Afterwards, the wall TUD_COMP-45 was re-tested up to light damage state and subsequently brought to near collapse state. The unstrengthened wall TUD_COMP-41 was tested under similar conditions for both the light damage and the near collapse state, but was not initially pre-damaged. To make a comparison in terms of serviceability limit state, the performance of wall TUD_COMP-45 before and after the strengthening should be considered; on the contrary, for the near collapse state the performance of strengthened wall TUD_COMP-45 and unstrengthened wall TUD_COMP-41 should be considered. To quantify the improved performance of the strengthened masonry, comparisons are made in terms of equivalent bilinear curve (Magenes et al. 2008, Morandi et al. 2018) and damage levels (Lagomarsino and Cattari 2015).

To study the performance of masonry strengthened with bed joint reinforcement against settlement, four-point bending tests on masonry wallets were performed (Figure 1a). These specimens represented the area below the window opening, which is the more prone to vertical cracks caused by settlement, shrinkage or expansion due to environmental conditions. Before the installation of the strengthening measure the wallets were neither pre-damaged nor tested.

For both the wall and the wallets the bed joint reinforcement was lay out as in practice; additionally diagonal ties were installed in the wall across existing diagonal stepwise cracks near the opening's corners (Figure 1a). Considering that the areas above and below the window opening are generally the most prone to settlement damage, often bed joint reinforcements are installed in these areas by placing one or two bars every two or three courses of masonry. For the wall and the wallets two twisted steel bars every three masonry courses were installed (green lines in Figure 1a). For the wall, one steel bars every five or six masonry courses was installed in piers that are defined as the vertical masonry portion next to the window opening (pink lines in Figure 1a). In addition, diagonal ties (blue lines Figure 1a) were placed in correspondence of the diagonal cracks to keep them as close as possible.

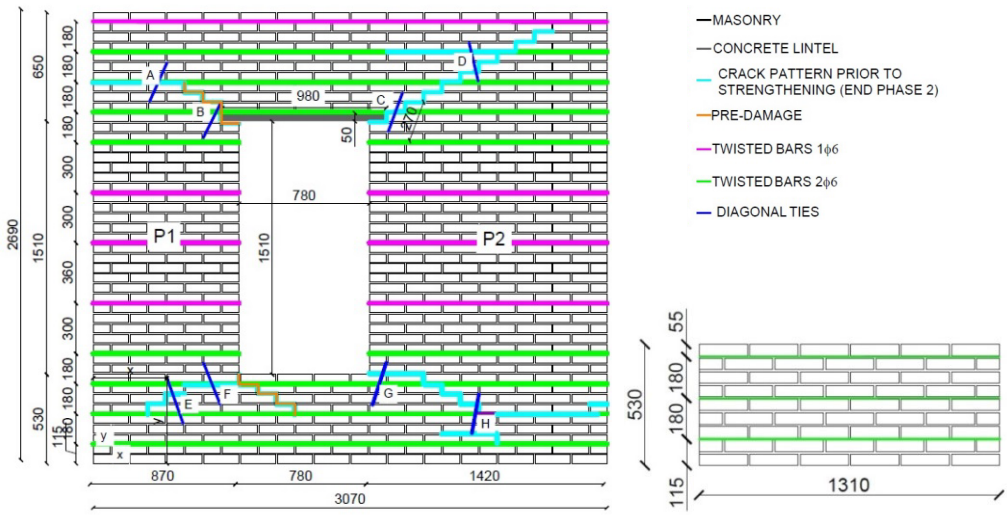

(a)

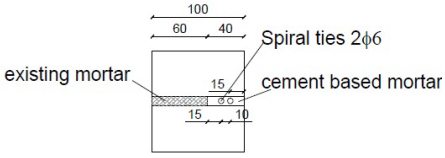

(b)

(c)

Figure 1. Overview of tested specimens: (a) dimensions and strengthening configuration; (b) detail of the strengthened bed joint; (c) execution of the intervention

2.2 ***Mechanical characterisation***

The specimens were made of solid clay bricks and built in running bond. The bricks had dimensions of 210 x 100 x 50 mm and the mortar used for construction had a *cement : lime : sand ratio* of 1 : 2 : 9. Table 1 lists the material properties of the single components and of masonry, while Table 2 lists the properties of the materials used for the strengthening, namely repair mortar, twisted steel bars and diagonal ties. The selected masonry type is representative of Dutch low-rise buildings constructed before 1945 (Jafari and Esposito 2017).

Since previous research showed that the bond behaviour between the twisted steel bars and the repair mortar plays an important role in the effectiveness of the strengthening method (Moreira et al. 2014), within this study pull-out tests have been performed to characterise the response of both twisted steel bars embedded in the repair mortar, and of the diagonal ties in the masonry. For the steel bars, six pull-out tests were performed in agreement with the standard EN 1766 (NEN 2015) by adopting auxiliary concrete cubes with dimensions 400 x 400 x 250 mm (Figure 2a). After the casting, three concrete cubes were cured in wet condition (under water) and the other three in dry condition (in air) in a conditioning room at (20 ± 2)° with 95% humidity for 28 days. For the diagonal ties, pull-out tests were performed on tie vertically installed in a masonry triplet with dimensions 210 x 170 x 100 mm (Figure 2b). The tests were performed by adopting the same set-up and testing procedure used by Skroumpelou et al. (2018). Monotonic pull-out tests were carried out for both specimens; additionally cyclic pull-out tests were performed for diagonal ties.

Table 1. Material properties of replicated clay brick masonry built in July 2018

Material property	Symbol	Average	C.o.V.	No. tests	Standard
Normalised compressive strength of masonry unit (210 x 100 x 50 mm)	f_b	28.31 MPa	0.10	9	EN 772-1 (CEN 2000)
Flexural strength of masonry unit	f_{bt}	6.31 MPa	0.11	8	NEN 6790 (NEN 2005)
Compressive strength of construction mortar (cement : lime : sand ratio of 1 : 2 : 9)	f_m	3.59 MPa	0.09	24	EN 1015-11 (CEN 1999)
Flexural strength of construction mortar	f_{mt}	1.55 MPa	0.10	12	
Density of masonry	ρ	1628 kg/m^3	0.01	-	
Compressive strength of masonry in the direction perpendicular to bed joints	f'_m	12.93 MPa	0.07	3	EN 1052-1 (CEN 1998)
Elastic modulus of masonry in the direction perpendicular to bed joints calculated between 1/3 and 1/10 of the maximum stress	E_3	3190 MPa	0.24		
Flexural bond strength	f_w	0.08 MPa	0.32	10	EN 1052-5 (CEN 2005)
Masonry initial shear strength	f_{v0}	0.13 MPa	-	6	EN 1052-3 (CEN 2002)
Masonry shear friction coefficient	μ	0.82	-		

For both the twisted bars and the diagonal ties slip and elongation of the bar occurred under monotonic tensile loading. In the case of the diagonal ties under cyclic loading, a similar behaviour was observed under tensile loading, while buckling and final rupture of

Table 2. Properties of the materials used for the strengthening

Material property	Symbol	Average	C.o.V.	No. tests	Standard
Cement-based repair mortar					
Compressive strength of repair mortar	$f_{m,r}$	46.42 MPa	0.09	16	EN 12190 (NEN 2018)
Flexural strength of repair mortar	$f_{mt,r}$	7.68 MPa	0.24	9	
Twisted steel bar *					
Ultimate tensile strength	f_{pu}	1112 MPa	-	-	
Tensile strength	F_{pu}	10 kN	-	-	
0.2% Proof stress	f_{py}	900 MPa	-	-	
Diagonal tie *					
Ultimate tensile strength	f_{pu}	1398 MPa	-	-	
Tensile strength	F_{pu}	13 kN	-	-	
0.2% Proof stress	f_{py}	1100 MPa	-	-	

** Data provided by producer*

(a) Diagonal ties *(b) Twisted steel bars*

Figure 2. pull-out test specimen

the tie was reported under compression loading. The results are reported in terms of pull-out stress versus relative displacement curve (Figure 3). For the cyclic tests, the envelope curve was calculated considering the force and the displacement in correspondence of the peak force and in correspondence of a drop of 20% of the maximum force (Skroumpelou et al. 2018). The curves in Figure 3 can be used as input for numerical analysis.

2.3 *Test set-up and loading scheme*

Figure 4 shows the set-up of the quasi-static cyclic in-plane test on a full-scale wall. Similarly to previous tests (Korswagen et al. 2017, Korswagen et al. 2018), the wall was built within a frame composed of a top and bottom steel beams and by two lateral

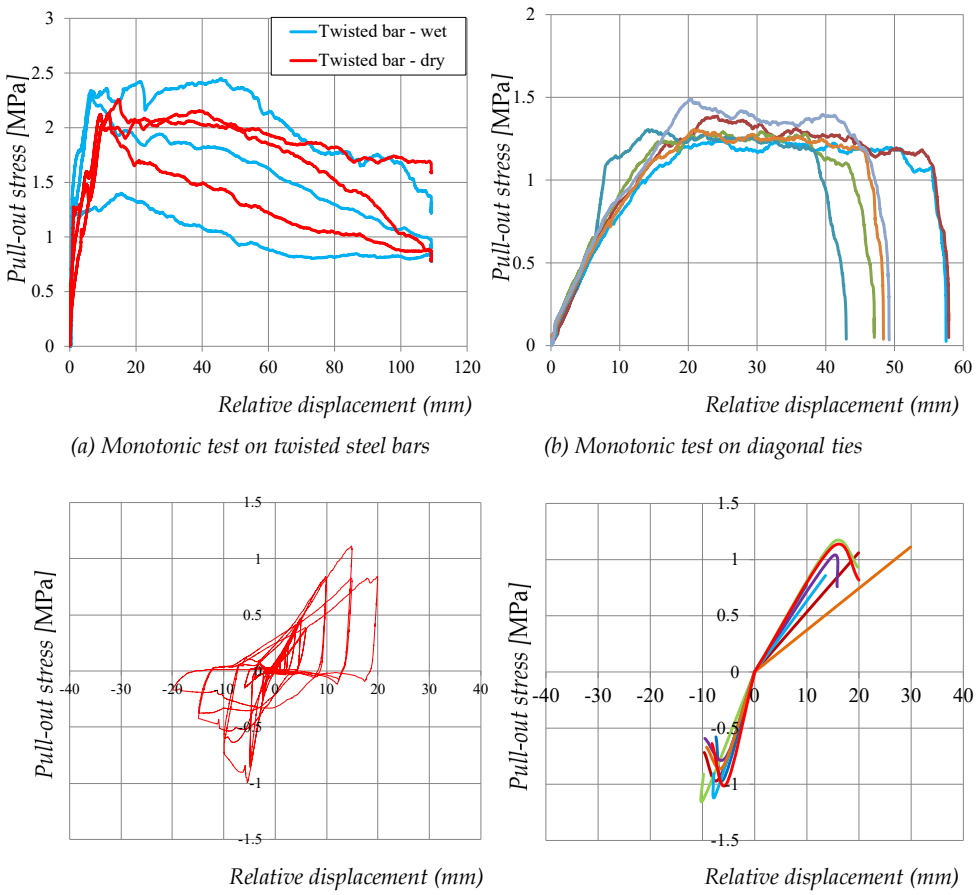

(a) Monotonic test on twisted steel bars *(b) Monotonic test on diagonal ties*

(c) Hysteretic curve cyclic test on diagonal tie *(d) Envelope curves cyclic tests on diagonal ties*

Figure 3. Pull-out stress versus relative displacement curve *Pull-out stress [MPa]*

columns. The first layer of bricks was glued to the bottom steel beam with "Sikadur 30" to avoid sliding at the base. The overburden was applied through two steel beams and was equal to 0.12 MPa. The bottom steel beam was connected to cross-beams which were fixed to the ground to prevent uplift. The lateral load was applied with a horizontal actuator with a capacity of 100 kN. The positive loading direction is defined when the horizontal actuator is compressed (from right to left in Figure 4) and the negative one when the actuator is extended. On the front side of the wall (which corresponds to the external side where the twisted steel bars were installed) the Digital Image Correlation (DIC) was applied; the backside of the wall (which corresponds to the internal side) was instrumented with contact sensors.

The walls were tested under a quasi-static cyclic lateral in-plane load in a cantilever configuration by controlling the horizontal displacement of the jack. The (actual) net horizontal displacement was calculated as the displacement of the top beam with respect to the external reference excluding possible rotations of the set-up and possible horizontal displacement of the bottom beam with respect to the external reference. The drift of the wall was calculated as the ratio between the net horizontal displacement and the height of the wall (Figure 1a). The lateral load was applied in three phases: phase 1 and phase 2 up to light damage with the same loading protocol as adopted in the study by Korswagen et al. (2018); phase 3 up to near collapse adopting a loading protocol representative for Groningen type earthquake. The latter was derived by means of a sensitivity numerical

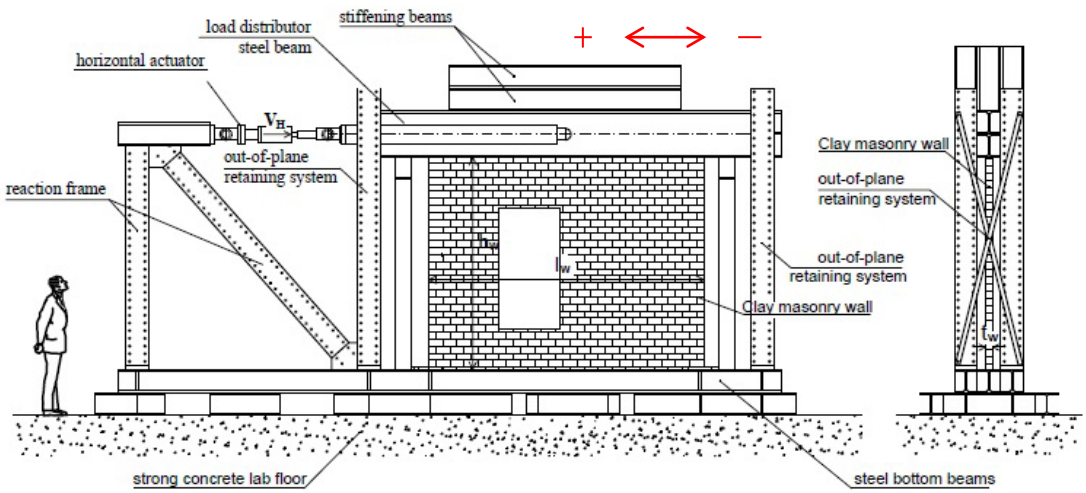

Figure 4. In-plane test set-up

study based on a full scale shaking table building test (Mariani 2016). In the light damage phases each cycle was composed of 30 runs, while in the near collapse phase the first two cycles were composed by two runs and the other cycles were composed by one run. In each phase a cycle is defined as the time interval in which the same target horizontal displacement was applied with the same rate, while a run is defined as the time needed to impose the target displacement in the positive and negative loading direction up to returning to the original position of the wall. During the light damage phase, the lateral load was applied with a constant rate equal to 0.125 mm/s; during the near collapse phase, the load-rate varied between 0.03 to 1 mm/s such that each cycle lasted 5 minutes (except for the last cycle that had to be stopped earlier because of out-of-plane deformation and lasted 4 min).

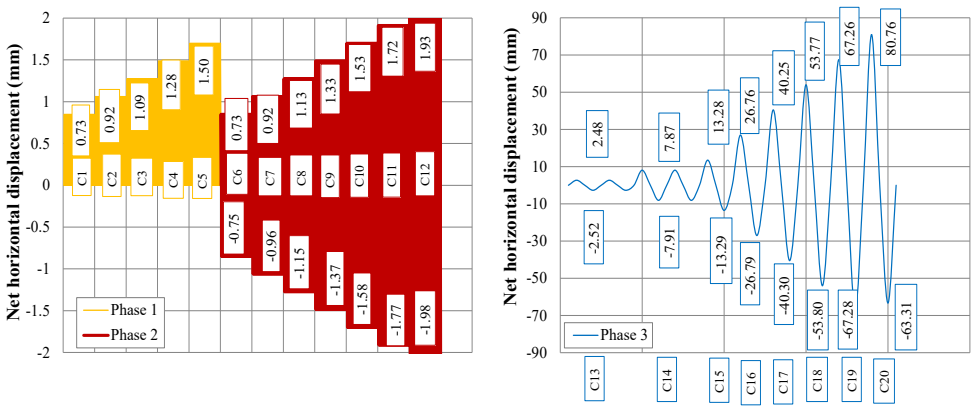

(a) Phase 1 and 2: light damage *(b) Phase 3: near collapse*

Figure 5. Loading scheme

Figure 6 shows the adopted set-up for the window bank test (four-point bending test), which is the same used in previous experimental campaign (Korswagen et al. 2017, Korswagen et al. 2018). To exclude the influence of the self-weight of the specimen a counterweight (CW1 and CW2) system was adopted. The counterweights (96 kg) were aligned with the hydraulic jacks on top, which had a capacity of 100 kN and were used to apply the load. The specimen was supported at the bottom by two rollers. The front side of the specimen, where the twisted steel bars were installed, was instrumented with DIC to detect crack initiation and propagation; the back part was instrumented with LVDTs to measure the vertical displacement and the crack width at the top of the specimen.

In the case of the unstrengthened wallets the test was performed by crack-mouth-opening control, while in the case of the strengthened wallets the vertical displacement of the jack was controlled. In the first case the crack mouth opening was chosen as controlling parameter in order to capture the quasi-brittle post-peak response; on the contrary in the second case this response was not observed allowing using the displacement control procedure. Both monotonic and cyclic tests were performed. The cyclic loading protocol consisted in three cycles composed of 30 runs (Figure 7) followed by a monotonic increase of the load up to failure. In the case of the unstrengthened wallets, the cycles were imposed at crack mouth opening (CMOD) equal to $w_1 = \frac{1}{4} w_c$, $w_2 = \frac{1}{2} w_c$ and $w_3 = \frac{3}{4} w_c$ of the crack mouth opening w_c corresponding to the peak force at point C (Figure 7a). In correspondence of point 1, 2 and 3 (Figure 7a) the ratio between the peak force F_i of each cycle and the maximum force F_c at point C (F_i / F_c) was found equal to 50%, 75% and 85%, respectively. Under monotonic loading, the strengthened specimen showed the transition between a flexural and a shear mechanism leading to the identification of two peak forces in the force versus displacement curve (point C and F). Considering this behaviour, the loading protocol was slightly modified by performing the first two cycles (C1 and C2) when the ratio between the applied force and the force at point C was equal to 50% and 75%, respectively, and the third cycle (C3) when the ratio between the applied force and the maximum force at point F was 85% (Figure 7b). Table 3 reports the loading scheme adopted for both unstrengthened and strengthened wallets.

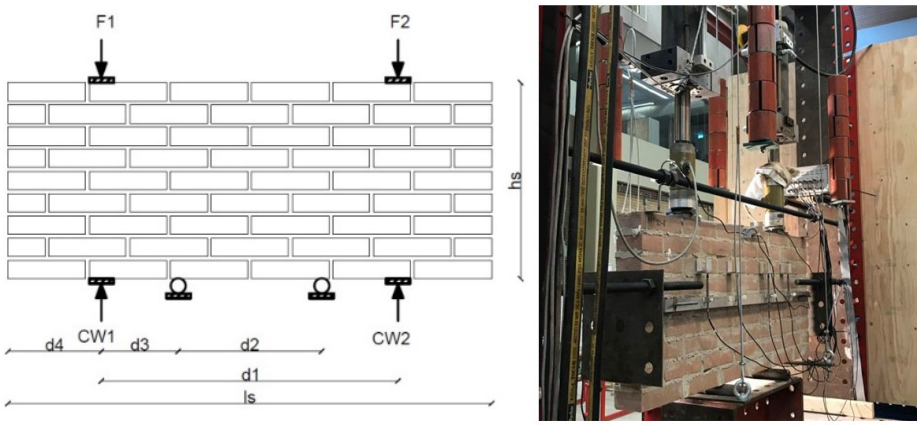

Figure 6. Window bank test set-up

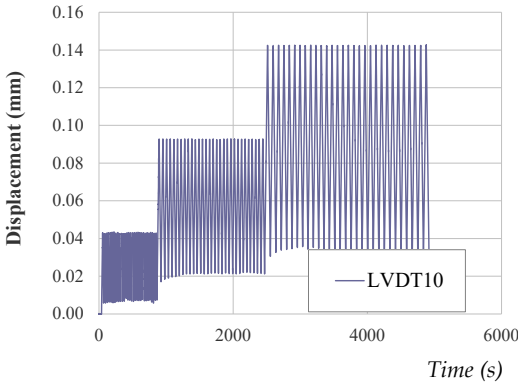

(a) Loading rate of unstrengthened specimens

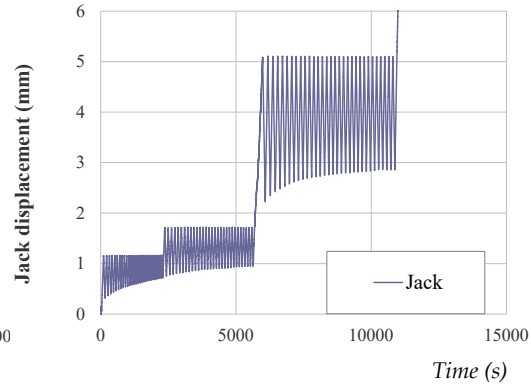

(b) Loading rate of strengthened specimens

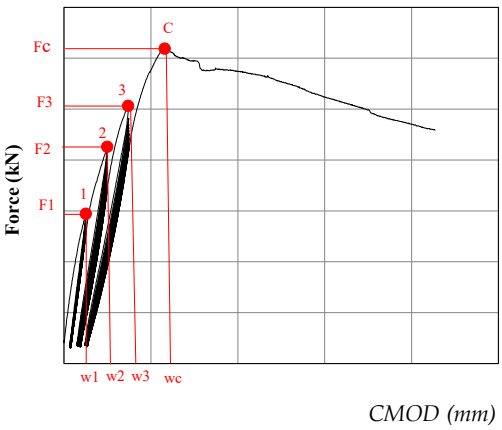

(c) Cyclic test of unstrengthened specimens

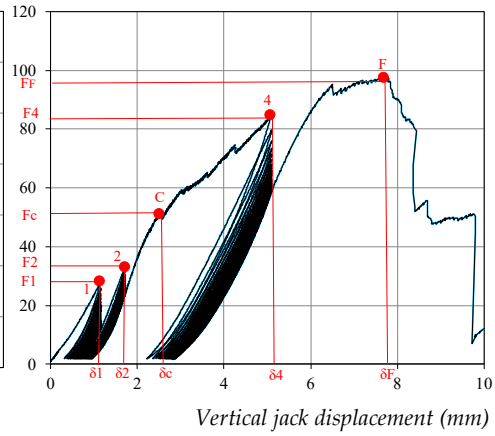

(d) Cyclic tests of strengthened specimens

Figure 7. Loading protocol

Table 3. Loading scheme for cyclic window bank test

			Unstrengthened CMOD control		Strengthened Jack displacement control	
Cycle	Run	CMOD mm	Force ratio	Rate mm/s	Force ratio	Rate mm/s
C1	1-30	$\frac{1}{4}w_c$	F_1 / F_c = 50%	0.00275	F_1 / F_c = 50%	0.015
C2	31-60	$\frac{1}{2}w_c$	F_2 / F_c = 75%	0.00275	F_2 / F_c = 75%	0.015
C3	61-90	$\frac{3}{4}w_c$	F_3 / F_c = 85%	0.00275	F_4 / F_F = 85%	0.030

3 Experimental results

3.1 In-plane test on full-scale wall

In this section, the results obtained from the in-plane test on the unstrengthened and strengthened walls are presented in terms of crack pattern and base shear force versus net horizontal displacement (Figure 8). The cracks are progressively numbered in order of occurrence.

The performance of the unstrengthened masonry is reported for wall TUD_COMP-45 (Korswagen et al. 2017, Korswagen et al. 2018) in the light damage phase and for wall TUD_COMP-41 (Korswagen et al. 2017, Korswagen et al. 2018, Messali 2018) in the near collapse phase. Both walls showed a similar behaviour in the light damage phase except for minor differences in the crack patterns that are highlighted by introducing the subscript "a" to the crack number for wall TUD_COMP-41. During Phase 1 (orange colour in Figure 8) crack number 1 and 2 developed diagonally from the bottom-right and the top-left opening's corner, respectively. During Phase 2 (red colour in Figure 8) crack number 3 and 4 propagated with a stepwise configuration from the bottom-left and the top-right corner of the window opening, respectively. During Phase 3 (blue colour in Figure 8), existing cracks further developed by increasing their width and length. At the end of phase 3 the cracks were mainly diagonal with a stepwise shape, starting from the window corner. Considering the first cycle of phase 1 (C1 d = 0.72 mm), the elastic stiffness was calculated as 29.06 kN/mm and 26.88 kN/mm for wall TUD_COMP-45 and TUD_COMP-41, respectively. The maximum base shear force of wall TUD_COMP-41 was equal to 22.05 kN (C4 d = 1.30 mm) and to -19.54 kN (C14 d = -7.97 mm) for the positive and negative loading direction, respectively. For wall TUD_COMP-41, the ultimate displacement was equal to approximately 40 mm in both loading directions, corresponding to a drift of 1.61/-1.49 %.

The performance of the unstrengthened masonry is reported for wall TUD_COMP-45, which was re-tested in the light damage phase after strengthening and then tested up to near collapse. During Phase 1 (orange colour in Figure 8), the stepwise crack number 1 at the bottom-right corner of the window opening re-opened; while at the top-left corner, crack number 2* occurred horizontally in a mortar joint where the reinforcement was not present. During phase 2 (red colour in Figure 8), crack number 3 and 4 re-opened and propagated diagonally from the bottom-left corner and top-right corner of the window opening, respectively. In phase 3 up to the same displacement at which the test for the

unstrengthened wall was stopped (C18, d = 53.77/-53.80 mm), a crack pattern composed of cracks staring at the window opening was observed, similarly to the unstrengthened wall. The following minor differences with the unstrengthened wall TUD_COMP-41 can be listed: stepwise cracks number 6a and 7a did not occur and an additional horizontal crack (number 8) was present on the wide pier P2. During cycle C18 (d = 53.77/-53.80 mm) horizontal cracks below the window opening occurred, probably caused by the formation of an arching mechanism induced by the reinforcement. The first sign of toe crushing consisting of vertical cracks in the bricks started during cycle C18 (d = 53.77/-53.80 mm) at the bottom-left and during cycle C19 (d = 67.26/-67.28 mm) at the bottom-right corner.

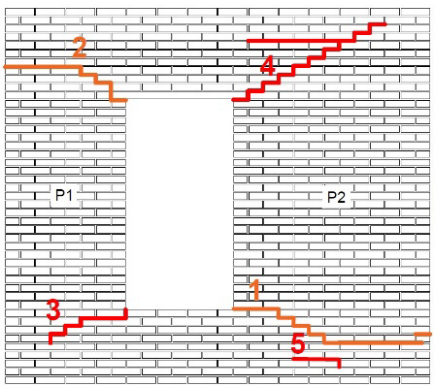

(a) Unstrengthened wall during the light damage phase 1 & 2

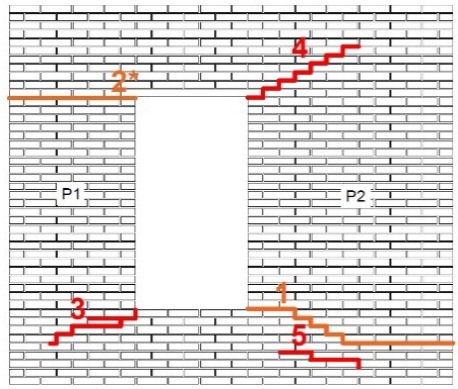

(c) Strengthened wall during the light damage phase 1 & 2

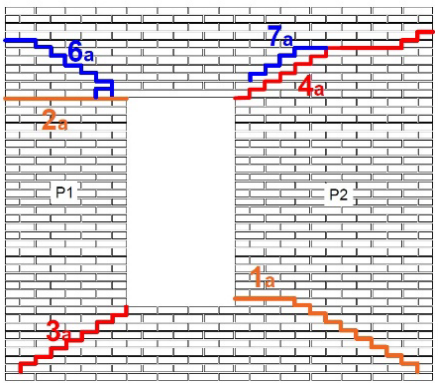

(e) Unstrengthened wall during the near collapse phase 3

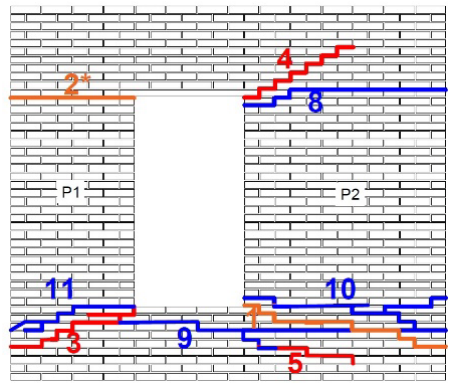

(g) Strengthened wall during the near collapse phase 3

Figure 8a. Crack patterns

Eventually, the test was stopped because excessive out-of-plane deformations were recorded. The strengthened wall showed an initial stiffness equal to 28.78 kN/mm (evaluated in C1 d = 0.73 mm) and a maximum base shear force was equal to 25.14 kN (C16 d = 23.08 mm) and -23.46 kN (C14 d = -7.90 mm) for the positive and negative loading direction, respectively. At the end of the near collapse phase, the ultimate displacement was equal approximately to 80 mm and to -60 mm for the positive and negative loading direction, corresponding to an ultimate drift of 2.99/-2.34 %.

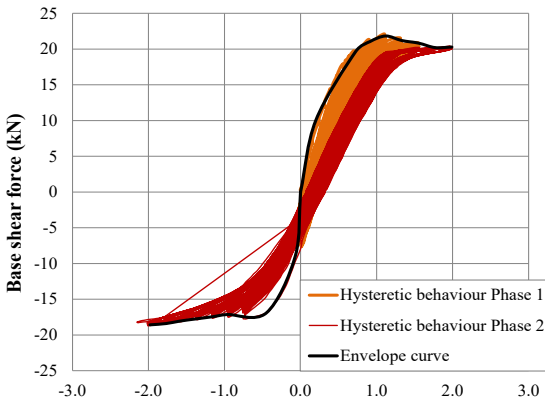

(b) Unstrengthened wall during the light damage phase 1 & 2

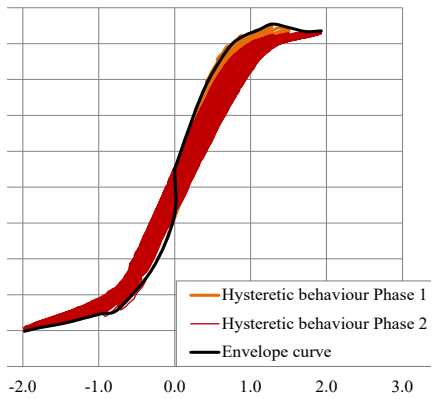

(d) Strengthened wall during the light damage phase 1 & 2

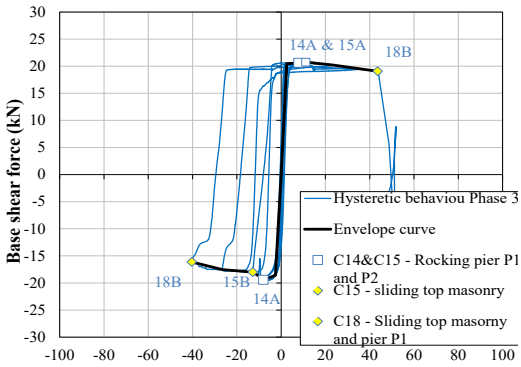

(f) Unstrengthened wall during the near collapse phase 3

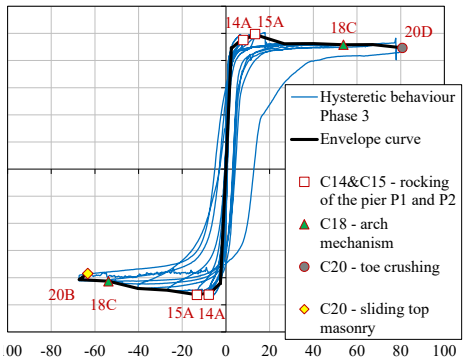

(h) Strengthened wall during the near collapse phase 3

Figure 8b. Base shear force versus net horizontal displacement curve
The positive loading direction is from left to right.

3.2 ***Window bank test***

In this section the results obtained from the cyclic test on unstrengthened (Korswagen et al. 2018) and strengthened wallets are presented in terms of force versus vertical displacement and crack evolution. The former has been obtained as the envelope curve of the cyclic curve.

Figure 9 shows the force versus the vertical displacement calculated considering the reading of LVDTs and the crack pattern evolution obtained through the DIC analysis. The envelope curves are reported and were calculated by considering the peak force in correspondence of each cycle. Relevant loads level were as follows: point A corresponds to the onset of cracking, point B corresponds to a force equal to 70 ÷ 75% of the force at point C, point C is defined as the peak force with flexure mechanism, point D refers to the failure for the unstrengthened specimen and to the transition to a shear mechanism for the strengthened wallets, point E corresponds to a force equal to 85% of the force at point F, and point F corresponds to the maximum force for the strengthened wallets obtained with a shear failure. In Figure 9, the comparison in terms of crack pattern is made by considering points A, C, D and F.

Considering the unstrengthened wallets, the force-displacement curve shows a linear behaviour up to the peak followed by an exponential softening curve; a flexural failure mechanism was observed. The first crack (point A) occurred in the head joints at the top of the masonry wallet and in the first bed joint at the bottom. Afterwards cracks in head and bed joints between the supports (in the constant moment zone) occurred leading to a flexural type failure. A maximum crack width of approximately 0.05 and 6.96 mm was observed at the peak force (point C) and at the end of the test (point D), respectively.

The strengthened wallets showed a transition from flexural to shear mechanism. Similarly to the unstrengthened wallets, at onset of cracking (point A) the first crack appeared in vertical head joints at the top of the specimen and in the last mortar bed joint at the bottom of the specimen. Afterwards the presence of small cracks in the joints located at the centre of the wallets lead to a slight reduction in stiffness up to point C, followed by a plateau up to point D. From point D cracks arose both in the joints and in the bricks forming diagonal shear-type cracks that lead to a substantial decrease in stiffness of the specimen up to the maximum force attained at point F. After point F a post-peak behaviour was recorded.

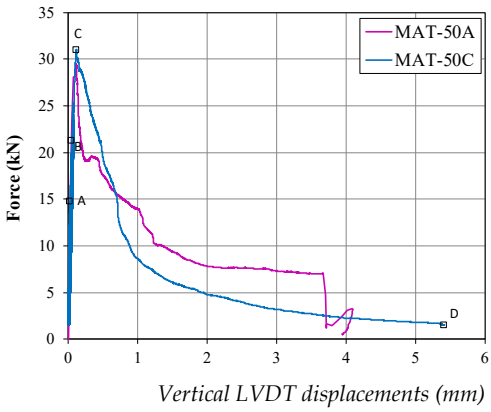

(a) Unstrengthened specimens

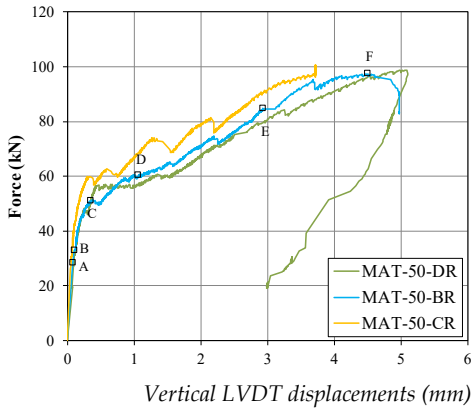

(b) Strengthened specimens

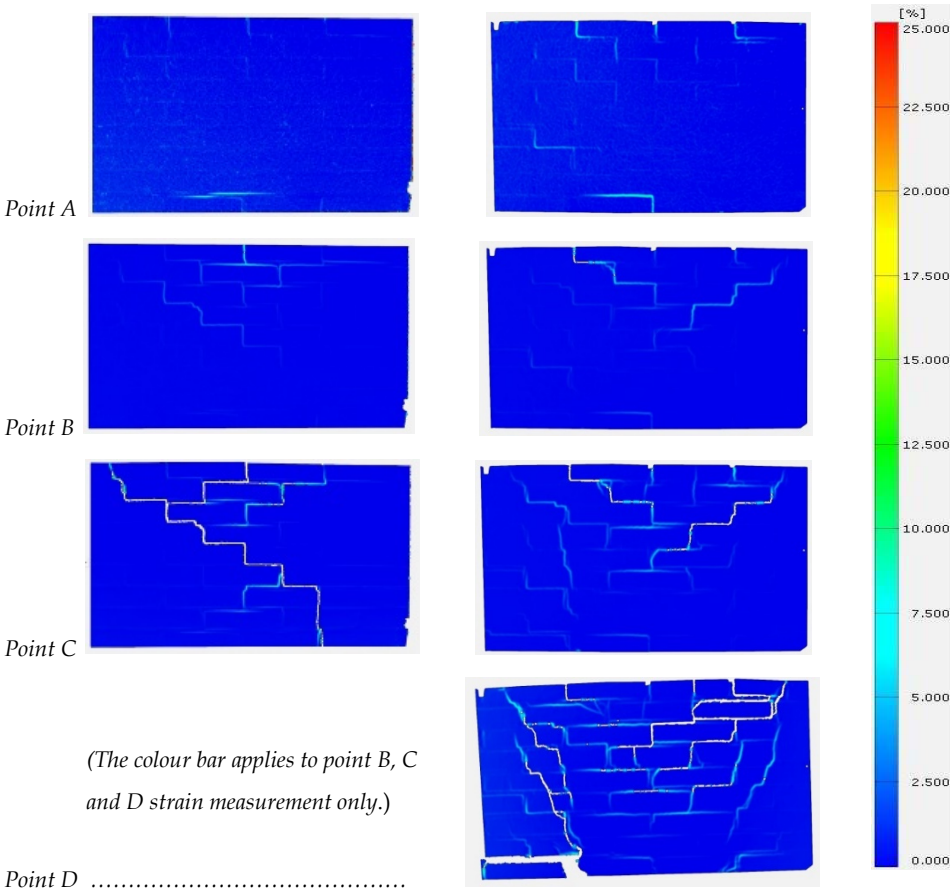

(The colour bar applies to point B, C and D strain measurement only.)

(c) Unstrengthened specimens

(d) Strengthened specimens

Figure 9. Force-displacement curve and crack pattern evolution observed during window bank tests

4 Discussion of the results

4.1 In-plane test on full-scale wall

In this section, the comparison between the unstrengthened and the strengthened wall is presented in terms of crack width and length for the light damage phase, and in terms of failure mechanisms, equivalent bilinear curve and damage levels for the near collapse phase.

At the end of the light damage phase (phase 2), the strengthened wall showed a reduction in (maximum) crack width between 20 and 25% and in crack length between 25 and 56% (Figure 10). These values were determined for cracks occurring at the same location and having similar shape. Consequently, the horizontal crack number 2* of the strengthened wall is not comparable with the stepwise crack number 2 of the unstrengthened wall, because this will results in misleading higher value of crack width. For both the unstrengthened and strengthened wall, the onset of cracking occurred at the same net horizontal displacement (C1, d = 0.73 mm).

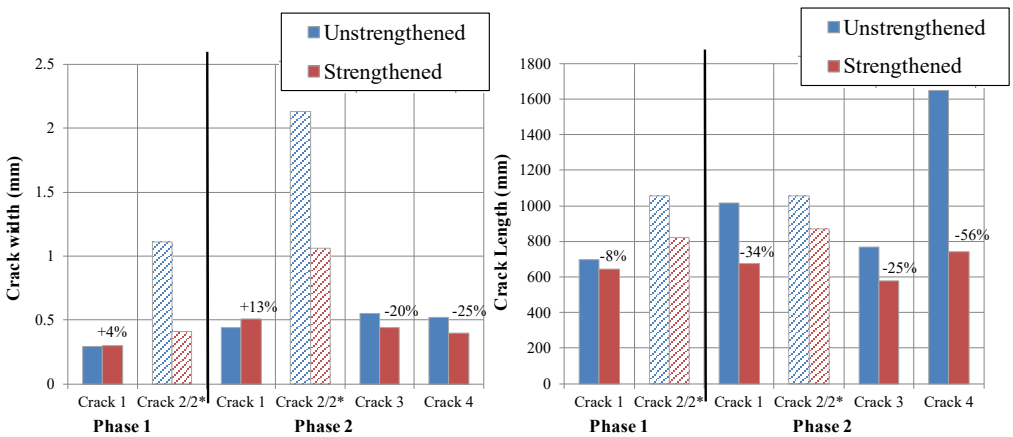

(a) crack width *(b) crack length*

Figure 10. Performance during light damage phase test in terms of crack with and crack length

Figure 11 shows the failure mechanisms of the masonry components during the near collapse phase (phase 3) for both unstrengthened and strengthened wall. Load levels associated to relevant mechanisms are marked in Figure 8, where point A refers to rocking of one of the piers, point B indicates sliding between two parts of the wall, point C refers to the formation of an arch mechanism below the window opening and point D indicates toe

crushing at the bottom of the wall. Considering the unstrengthened wall, until cycle C14 (d = 7.89/-7.97 mm) the rocking of the piers was the prevailing mechanisms in both loading directions (point 14-A, Figure 8f). During cycle C15 (d = -12.82 mm) sliding of the top masonry portion occurred with respect to both piers in the negative loading direction (point 15-B, Figure 8f), while rocking of the piers was the prevailing mechanism for the positive loading direction. During cycle C18 (d = 43.63 mm) for positive loading (point 18-B, Figure 8f), the L-shaped portion of masonry composed of the top part of the wall and pier P2 started to slide with respect to the remaining parts of the wall. This led to the loss of integrity of the wall and to the consequent termination of the test. Initially, the strengthened wall showed a behaviour similar to the unstrengthened one with rocking of the piers in both loading directions (points 14-A and 15-A, Figure 8h). During cycle C18 (d = 53.77/-53.80 mm) horizontal cracks occurred in the masonry portion below the window opening and a small uplift of the central bricks was observed. This suggests the formation of an arch mechanism caused by the activation of the twisted steel bars embedded in the bed joints (point 18-C, Figure 8h). Thanks to the ability of the bed joint reinforcement to keep the integrity of the wall, larger net horizontal displacement could be attained for the strengthened wall with respect to the unstrengthened one. During cycle 20 (d = 80.96/-63.31 mm) toe crushing (Figure 12a) of the bottom right corner (point 20-D, Figure 8h) and sliding of the top masonry portion with respect to the piers (point 20-B, Figure 8h) occurred in positive and negative loading direction, respectively.

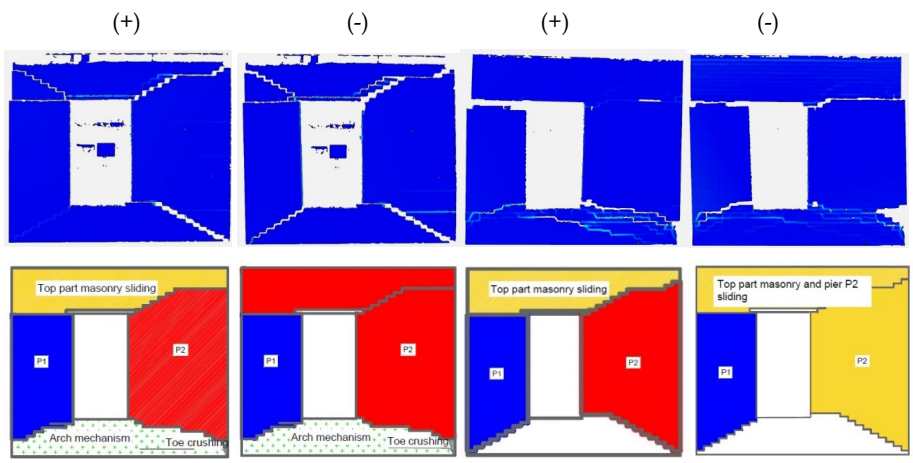

(a) unstrengthened *(b) unstrengthened* *(c) strengthened* *(d) strengthened*

Figure 11. Relevant failure mechanism observed through DIC analysis at the end of the near collapse phase (phase 3)

Differently than for the unstrengthened wall, the strengthened wall showed excessive out-of-plane deformation of the piers (Figure 12b), which lead to the termination of the test. Figure 13 shows the out-of-plane deformation versus the net horizontal displacement for the unstrengthened (blue triangles) and strengthened wall (red circles). The unstrengthened wall was subjected to an out-of-plane deformation of 10 mm in the last cycle (cycle C18). Considering the strengthened wall, the out-of-plane deformation was similar to the one observed for the unstrengthened wall up to cycle C15, especially for the narrow pier P1. In correspondence of the last cycle (C20, d = -63 mm) both piers showed a significant out-of-plane deformation of approximately 40 mm for the negative loading direction. This out-of-plane deformation can be attributed to the asymmetric position of the twisted steel bars in the thickness of the wall (Figure 1b) and to the difference in stiffness between the repair and the construction mortar.

To compare the seismic performance of the unstrengthened and strengthened wall, the equivalent bilinear curve was calculated (Magenes et al. 2008, Morandi et al. 2018) (Figure 14). The strengthened wall showed a slight increment in force capacity (+15%) and a significant increment in terms of displacement capacity (+40 ÷ 45%) and ductility (+30 ÷ 40%). Both walls show a limited reduction in force capacity after reaching its maximum value; this is consistent with the rocking or sliding failure mechanism observed in both walls.

To compare the evolution of damage and failure mechanisms in the near collapse testing phase, damage levels were defined coupling qualitative observations on the type of

(a) *(b)* *(c)*

Figure 12. Photos of failure mechanisms for the strengthened wall at the end of the near collapse phase (C20 d = 80.96/63.31 mm): (a) toe crushing of the bottom-right corner, (b) cracks in the brick at bottom-right corner; (b) out-of-plane of the pier P1 and cracks in the brick at bottom-left corner

damage and quantitative information on the residual drift $d_{r,res}$. Four damage levels were considered (Lagomarsino and Cattari 2015): DL1 associated to no visible damage (by naked eye), DL2 identifying minor damage, DL3 associated to moderate damage, DL4 identifying extensive damage. The residual drift was calculated as the permanent deformation after a hysteretic cycle. Figure 15a shows the residual drift versus the maximum absolute drift, which is calculated considering the maximum drift in positive or negative loading direction for each cycle. Following the work by Lagomarsino and Cattari (2015), the normalised (with respect to

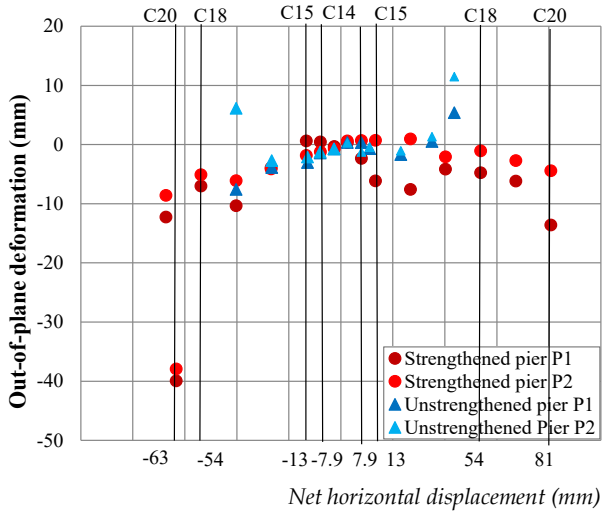

Figure 13. Out-of-plane deformation

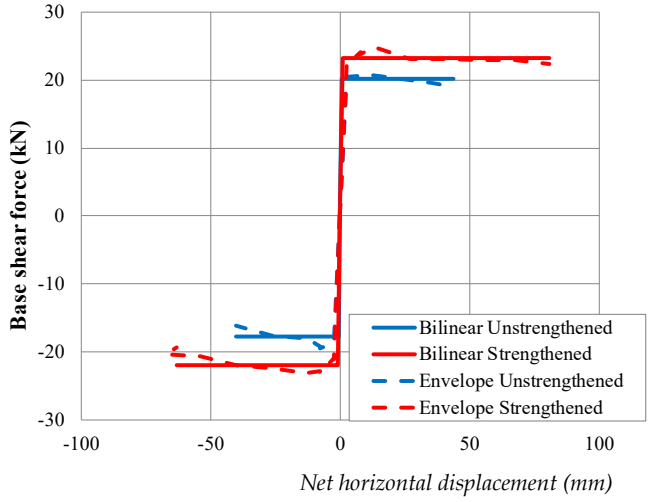

Figure 14. equivalent bilinear curve

the maximum value) base shear force k_G and the drift d_r are provided for each damage level (Table 5). Figure 15b shows a representation of the damage levels on the envelope curve. The damage level DL1, no visible damage, was defined for a maximum crack width equal to 0.1 mm recorded by DIC analysis; this limit was considered to be representative of cracks not visible at naked eye (Burland and Wroth 1974, Boscardin and Cording 1989). For both the unstrengthened and the strengthened wall, damage level DL1 is identified in correspondence of cycle C1 (d = 0.73 mm). The damage level DL2, minor damage, was defined for a residual drift equal to 0.01 when the cracks (number 1 - 4) were fully developed from the corner's opening to the corners of the wall up to a maximum crack width approximately equal to 2 mm. The damage level DL3, moderate damage, was associated to significant residual drift equal to 0.1%. The damage level DL4, extensive damage, was defined for a residual drift equal to 1% or in correspondence of significant out-of-plane deformation. Figure 15c shows the comparison for the unstrengthened and strengthened wall in terms of maximum absolute drift at which a certain damage level is attained. Considering DL1 and DL2, the maximum absolute drift is similar for both walls; considering DL3 and DL4, the damage state occurred at larger maximum absolute drift in the strengthened wall with respect to the unstrengthened one, meaning that the presence of the bars delayed the failure mechanisms. By comparing the results with the one obtained by Lagomarsino and Cattari (2015) (Table 5 and Figure 15d), a good agreement is found for damage level DL1 and DL2 for both walls. For damage level DL3, the unstrengthened wall shows comparable values of normalised base shear force and drift, while the strengthened wall shows higher values. For both the unstrengthened and strengthened wall, damage level DL4 is identified for higher values of normalised base shear and drift. For the unstrengthened wall the difference can be due to the fact that

Table 4. Parameter of the bilinear curve

Parameter	Unit	Unstrengthened		Strengthened	
		Neg.	Pos.	Neg.	Pos.
K_{el}	kN/mm	24.73	28.06	27.02	27.98
u_u	mm	-40.3	43.63	63.30	80.76
V_u	kN	-17.67	20.10	-21.90	23.17
u_{el}	mm	-0.72	0.72	-0.94	0.98
μ_b	-	56.4	60.9	78.1	97.5
d_{r-b}	%	-1.49	1.61	-2.34	2.99

within this study a single wall was considered, while Lagomarsino & Cattari (2015a) refers to a wide category of heritage masonry structures characterised by less ductile shear mechanisms. Additionally, although the presented wall has an opening, it is here considered as a single macroelement, while according to the subdivision by Lagomarsino and Cattari (2015) it will be composed by multiple macroelements. In the study by Lagomarsino and Cattari (2015) only unstrengthened masonry structures were considered, consequently it is logical to obtain higher values of normalised shear force and drift for the strengthened wall. Nevertheless this preliminary comparison can set the basis for further studies on the definition of normalised base shear force and drift for strengthened elements.

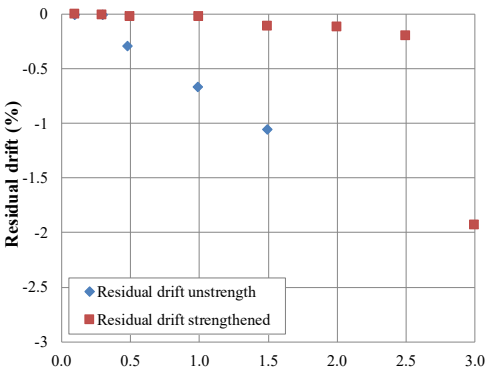

Maximum absolute drift (%)

(a) Residual drift versus absolute drift

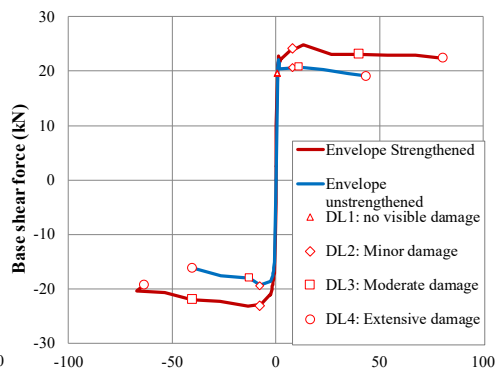

Net horizontal displacement (mm)

(b) Representation of the damage levels on the envelope curve

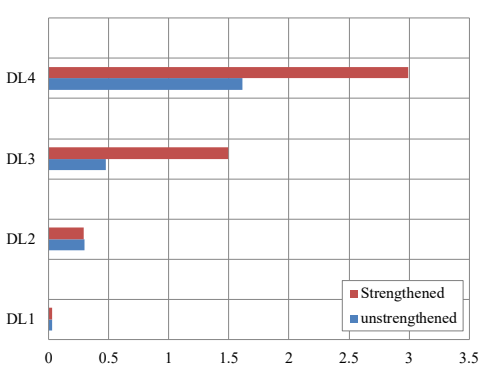

Maximum absolute drift (%)

(c) Comparison in terms of absolute drift

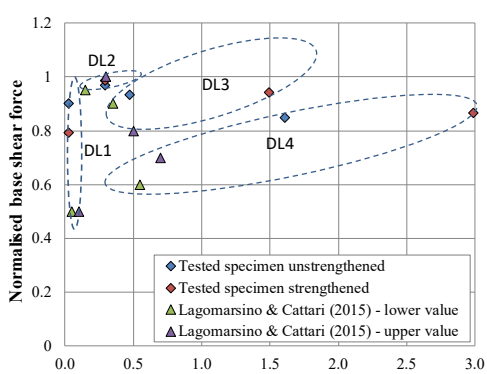

Maximum absolute drift (%)

(d) Comparison with the values obtained by Lagomarsino and Cattari (2015)

Figure 15. Definition of the damage levels

Table 1 - Identification of the damage levels and comparison with the values proposed by Lagomarsino and Cattari (2015)

Damage Level		Criteria	Tested Specimen						Lagomarsino and Cattari (2015)	
			Unstrengthened			Strengthened				
		$d_{r,res}$	k_G	d_r	d	k_G	d_r	d	k_G	d_r
				%			%			%
DL1	No visible damage: maximum crack width equal to maximum 0.1 mm	-	0.90	0.03	0.72	0.79	0.03	0.73	>0.50	0.05-0.10
DL2	Minor damage. Diagonal crack further developing from the window corner	0.01	0.94	0.29	7.89	0.97	0.29	7.87	0.95-1.00	0.15-0.30
			1	-0.29	-7.97	0.99	-0.29	-7.90		
DL3	Moderate damage. Starting to have residual drift	0.1	0.94	0.41	11.11	0.93	1.49	40.25	0.80-0.90	0.35-0.50
			0.92	-0.47	-12.82	0.94	-1.49	-40.29		
DL4	Extensive damage, not economically sustainable. Out-of-plane deformation of the piers	1	0.86	1.61	43.63	0.90	2.99	80.76	0.60-0.70	0.55-0.70
			0.83	-1.49	-40.29	0.83	-2.34	-63.31		

4.2 *Window bank test*

In this section the comparison between the unstrengthened and strengthened wallets is carried out in terms of flexural strength, elastic modulus, crack width and load at onset of cracking. The presence of the twisted steel bars led to a transition between a flexural to a shear mechanism for the strengthened wallets, bringing to the attainment of two peaks in the force-displacement curve, point C and point F (Figure 9). Consequently, to compare the unstrengthened and the strengthened wallets for the same failure mechanism the properties were calculated with respect to point C.

Table 6 lists the values of the mechanical properties of the unstrengthened and strengthened wallets. It can be observed that the presence of the steel bars caused an increase of the flexural strength $f_{x3,c}$ approximately of 35% and a decrease in the elastic modulus $E_{fx3,c}$, calculated as the chord modulus between 1/10 and 1/3 of $f_{x3,c}$, of 35%.

In terms of crack width, the comparison is made considering the crack in the central vertical head joint at the top of the wallet for the load levels at point A and C (Table 7). It can be observed that for the unstrengthened specimens, the first crack occurred at a load of 15 kN and for the strengthened ones at a load of 28 kN that is an increment of approximately 47%. At a load of 31.01 kN, unstrengthened wallet reached its maximum

Table 6. Bending properties of strengthened and unstrengthened cyclically loaded masonry specimens

	Unstrengthened				Strengthened		
Name	F_c	$f_{x3,c}$	$E_{fx3,c}$	Name	F_c	$f_{x3,FC}$	$E_{3,FC}$
	kN	MPa	MPa		kN	MPa	MPa
MAT-50A	29.47	0.64	3719	MAT-50BR	55	1.20	2069
MAT-50C	31.01	0.66	3377	MAT-50CR	40	0.84	2499
				MAT-50DR	41	0.89	2157
Average	30.24	0.65	3548	Average	45.33	0.98	2242
St. dev.	0.77	0.01	171	St. dev.	6.85	0.16	185
C.o.V.	0.025	0.02	0.05	C.o.V.	0.15	0.16	0.08
Difference						+35%	35%

capacity (point C) and showed a maximum crack width equal to 0.05 mm; at the same force level the strengthened wallets show a crack width equal to 0.03 mm, that is a reduction of approximately 40%.

Table 7. Width of vertical crack in the head joint centrally located on the top side of the wallets

	Unstrengthened (MAT-50C.)		Strengthened (MAT-50BR.)	
	Force [kN]	Crack width [mm]	Force [kN]	Crack width [mm]
Point A	15.00	0.05	28.20	0.05
Point C	31.01	0.05	51.07	0.08
Difference			+47%	-40%

5 Concluding remarks

In the Netherlands, the reinforced repointing, also known as bed joint reinforcement, is often used as repair or strengthening measure for historical unreinforced masonry buildings due to its limited invasiveness and ability to preserve the aesthetic aspect of buildings. It was often used against damage caused by settlement or shrinkage; however, recently the question arose if this strengthening measure can be used against low-intensity induced earthquakes, which arose in the north part of the Netherlands (Groningen area) due to gas extraction. Therefore, it is of interest to investigate the performance of masonry strengthened with bed joint reinforcement both against settlement and seismic loading. To this purpose, an experimental campaign was conducted at Delft University of Technology, including four-point bending tests on masonry wallets a quasi-static test on a full-scale wall and companion material characterisation tests. To this end, results and specimens of previous research focusing on low-rise unreinforced masonry buildings were considered (Jafari and Esposito 2017, Korswagen et al. 2017, Korswagen et al. 2018, Messali 2018).

Consequently, the results obtained in this study represent a preliminary investigation and different response could be observed for specimens more representative of historical buildings (e.g. multi-wythe walls). They also provide the basis for numerical studies (Drougkas et al. 2020a, Drougkas et al. 2020b).

Regarding the effectiveness of the bed joint reinforcement against seismic loading, the following conclusions can be drawn from quasi-static cyclic in-plane tests:

- In the unstrengthened wall the cracks mainly developed diagonally from the window corners with a stepwise configuration. The presence of the bars led to a different cracks pattern for the strengthened wall: in the masonry portion above the window opening the cracks developed horizontally in mortar joints where the reinforcement was not present; in the masonry portion below the window opening the cracks developed in the mortar joints forming an arch mechanism. At the end of the test for displacement larger than the one reached for the unstrengthened wall, the cracks occurred also in the bricks at the bottom corners of the wall leading to toe crushing.
- At the end of the light damage phase, crack width (-20 ÷ 25%) and length (-25 ÷ 55%) reduction were obtained.
- During the near collapse phase, a significant increment in displacement capacity (+40 ÷ 45%) and in ductility (+30 ÷ 40%) was observed; the increment in terms of maximum base shear force was limited (+15%). The increase in displacement capacity is manly to be attributed to the ability of the strengthening method to avoid separation of the wall in different piers. These results are in line with the ones obtained for unreinforced brick masonry piers strengthened with textile reinforced mortar (Kouris and Triantafillou 2018).
- The presence of the bars leads also to a different evolution of the failure mechanisms. In the unstrengthened wall the prevailing mechanisms were rocking of the pier and sliding of a portion of the masonry wall with respect to the rest of the wall. The strengthened wall initially showed similar mechanisms observed for the unstrengthened wall, but for larger displacement an arch mechanism was observed below the window opening and toe crushing occurred; a significant out-of-plane deformation, possibly caused by the asymmetric position of the steel bars in the thickness of the wall, was observed at the end of the test.

Regarding the effectiveness of the bed joint reinforcement against the formation of vertical cracks due to i.e. settlement, the following conclusions can be drawn from four-point bending tests:

- The presence of the bars leads to a transition from a flexural to a shear failure mechanism.

- An increment of flexural strength (+35%) and a reduction of the elastic modulus (-35%) was observed.
- An increase of load at onset of cracking was obtained (+47%).
- A reduction of crack width (-40%) was achieved.

In conclusion, the presence of the bars leads to a more ductile behaviour and to an increased displacement capacity. Furthermore, it contributes to delay the crack process and to reduce the crack width and length. Although the aforementioned outcomes are based on a limited number of tests and further investigations are needed, the bed joint reinforcement can be considered as a promising non-invasive strengthening measure against subsidence-induced damage as the one provoked by settlement and low-intensity earthquakes.

Acknowledgements
This research was found by the Rijksdienst voor het Cultureel Erfgoed (RCE), part of the Ministerie van Onderwijs, Cultuur en Wetenschap (OCW), which is gratefully acknowledged. Subsidy number MS-2018-189.

References

Boscardin, M. D. and E. J. Cording (1989). Building response to excavation-induced settlement. *Journal of Geotechnical Engineering* 115(1): 1-21.

Burland, J. B. and C. Wroth (1974). *Settlement of buildings and associated damage. Conference on Settlement of Structures*, Cambrige (UK), Pentech press.

CEN (1998). EN 1052-1 - Method of test masonry – Part 2: Determination of compressive strength. Brussels, Belgium, European Committee for Standardisation.

CEN (1999). EN 1015-11 - Method of test for mortar for masonry – Part 11: Determination of flexural strength of hardened mortar. Brussels, Belgium, European Committee for Standardisation.

CEN (2000). EN 772-1 - Methods of test for masonry units - Part 1: Determination of compressive strength. Brussels, Belgium, European Committee for Standardisation.

CEN (2002). EN 1052-3 - Method of test masonry – Part 3: Determination of initial shear strength. Brussels, Belgium, European Committee for Standardisation.

CEN (2005). EN 1052-5 - Method of test masonry – Part 5: Determination of bond strength by bond wrench method. Brussels, Belgium, European Committee for Standardisation.

Drougkas, A., L. Licciardello and R. Esposito (2020a). Experimental testing and numerical analysis of strengthened historic masonry subjected to induced seismicity. *11th International Conference on Structural Dynamics*, Athens, Greece

Drougkas, A., L. Licciardello, J. G. Rots and R. Esposito (2020b). In-plane seismic behaviour of retrofitted masonry walls subjected to subsidence-induced damage. *Engineering Structures* 223: 111192.

Ismail, N., R. B. Petersen, M. J. Masia and J. M. Ingham (2011). Diagonal shear behaviour of unreinforced masonry wallettes strengthened using twisted steel bars. *Construction and Building Materials* 25(12): 4386-4393.

Jafari, S. and R. Esposito. (2017). Material tests for the characterisation of replicated solid clay brick masonry. Report No. C31B67WP1-12. Delft University of Technology

Kallioras, S., G. Guerrini, U. Tomassetti, B. Marchesi, A. Penna, F. Graziotti and G. Magenes (2018). Experimental seismic performance of a full-scale unreinforced clay-masonry building with flexible timber diaphragms. *Engineering Structures* 161: 231-249.

Korswagen, P., M. Longo and E. Meulman. (2017). Damage sensitivity of Groningen masonry structures – experimental and computational studies, Delft University of Technology

Korswagen, P., M. Longo and E. Meulman. (2018). Damage sensitivity of Groningen masonry structures – experimental and computational studies, Delft University of Technology

Kouris, L. A. S. and T. C. Triantafillou (2018). State-of-the-art on strengthening of masonry structures with textile reinforced mortar (TRM). *Construction and Building Materials* 188: 1221-1233.

Lagomarsino, S. and S. Cattari (2015). PERPETUATE guidelines for seismic performance-based assessment of cultural heritage masonry structures. *Bulletin of Earthquake Engineering* 13(1): 13-47.

Licciardello, L. and R. Esposito. (2020). Experimental study on unreinforced masonry strengthened with bed joint reinforcement. Report No. CM1B07-2. Delft University of Technology

Licciardello, L., J. G. Rots and R. Esposito (2021). Performance of unreinforced masonry strengthened with bed joint structural repointing. *12th Conference on Structural Analysis of Historical Construction*, Barcelona, Spain.

Magenes, G., P. Morandi and A. Penna (2008). In-plane cyclic tests of calcium silicate masonry walls. *14th International Brick/Block Masonry Conference*, Sydney, Australia.

Mariani, V. (2016). Sensitivity studies of the shaking table test on EUC-BUILD-2. Delft University of Technology

Messali, F. (2018). Test results of wall TUD_COMP-41 under near collapse protocol. L. Licciardello and R. Esposito.

Morandi, P., L. Albanesi, F. Graziotti, T. Li Piani, A. Penna and G. Magenes (2018). Development of a dataset on the in-plane experimental response of URM piers with bricks and blocks. *Construction and Building Materials* 190: 593-611.

Moreira, S. M. T., L. F. Ramos, B. Csikai and P. Bastos (2014). Bond behaviour of twisted stainless steel bars in mortar joints. *9th International Masonry Conference* Proceedings, Guimaraes, Portugal.

NEN (2005). NEN 6790 - Technical principles for building structures-TGB 1990- Masonry structures- Basic requirements and calculations methods. Delft, The Netherlands, Nederlands Normalisatie-instituut.

NEN (2015). NEN 1766 - Products and systems for the protection and repair of concrete structures -Test methods – Reference concrete for testing. Delft, The Netherlands, Nederlands Normalisatie-instituut.

NEN (2018). NEN 12190 Products and systems for the protection and repair of concrete structures - Test methods - Reference concrete for testing. Delft, The Netherlands, Nederlands Normalisatie-instituut.

NIKER. (2010). Critical review of retrofitting and reinforcement techniques related to possible failure. Report No. Deliverable 3.2.

Skroumpelou, G., F. Messali, R. Esposito and J. G. Rots (2018). Mechanical characterization of wall tie connection in cavity walls. *10th Australian Masonry Conference*, Sydney, Australia.

Valluzzi, M. R., L. Binda and C. Modena (2005). Mechanical behaviour of historic masonry structures strengthened by bed joints structural repointing. *Construction and Building Materials* 19(1): 63-73.